

Direct observation of electrostatic charging in 3D printing

Received: 9 February 2024

Accepted: 22 June 2025

Published online: 19 August 2025

Ezequiel Lorenzetti ¹, Yan A. S. da Campo ², Milton A. F. Neto ³ & Thiago A. L. Burgo ^{1,2,3} ✉

The spontaneous electrification of surfaces and interfaces is a widespread phenomenon that produces unexpected effects in chemical reactivity and mass charge transfer, revealed in abundant literature over the past twenty years. The pervasive presence of electrostatic charges originates from many sources, including friction, mechanochemical reactions, phase change, flexoelectricity, and others. Since fused deposition modeling undergoes most well-known electrification mechanisms, it would be not surprising that 3D-printed objects display large amounts of charge. Here we uncover the hitherto unexplored realm of electrostatic charging in 3D printing, underscores the impact of printing parameters on charge generation in polymers. Substrates, printing speed, temperature, and printing direction each exert distinct impacts on charge buildup, depending upon the material used for printing. We also develop simple protocols employing common multimeters for charge monitoring, while substrates subjected to corona charging or triboelectrification demonstrate effective methods for charge control or mitigation. An original development is achieved by demonstrating the ability to print quasi-electrets, indicating a potential revolution in electret technology. The implications of these findings establish the groundwork for advancements in 3D printing technology and electrostatics, creating new scientific opportunities for a better understanding of matter.

Electrostatic charges have an inherent nature of being discrete, invisible, and unpredictable¹. These are probably the reasons why so many scientists and engineers often invoke the Electroneutrality Principle², where bulk matter is conveniently assumed as electrically neutral. On the other hand, for most systems (and even pure isolated substances) the widespread belief in electroneutrality is hardly verified^{3,4}. As the result of steady state charge dissipation rates, even materials carrying a net charge close to zero frequently display stable mosaics of fixed positive and negative charges^{5–7}, reaching electrostatic potential gradients as high as 20 kV m^{−1}. Extensive literature^{8–22}, has shown that electrostatic charges are ubiquitous in all real systems, regardless of whether they are natural or anthropic ones.

The difficulty to predict, detect and identify electrostatic charges (mainly on dielectric insulators) is the root of many undesirable situations and large-scale property losses: damage of electronic equipment^{23–27}, unwanted adhesion during the processing, bulking and shipping of powder^{28–32}, and serious industrial accidents and explosions^{33–35}. Despite the hazards and problems triggered by electrostatic discharge, electrostatic charging plays a central role in many important technologies such as photocopying^{36,37}, electrostatic painting³⁸, electrospinning^{39–41}, electrets^{42–45}, and electrostatic precipitators/separators^{46,47}.

Contact electrification (CE) is one of the main causes of systems that have a net electrostatic charge, and it is expected whenever two

¹Department of Chemistry and Federal University of Santa Maria. Av. Roraima, 1000, Santa Maria, RS 97105-900, Brazil. ²Department of Physics, Federal University of Santa Maria. Av. Roraima, 1000, Santa Maria, RS 97105-900, Brazil. ³Department of Chemistry and Environmental Sciences, Ibilce, Sao Paulo State University (Unesp), R. Cristovao Colombo, 2265, S. J. Rio Preto, SP 15014-100, Brazil. ✉e-mail: thiago.burgo@unesp.br

surfaces are brought into contact^{48–50}. Although CE is commonly associated with the solid-solid contact^{5,6,51}, charge transfer is a universal phenomenon and most interfaces are important sites for electric charge accumulation and exchange⁵². In fact, liquid-liquid^{53–57}, liquid-solid^{58–63}, gas-liquid⁶⁴ and gas-solid⁶⁵ systems can develop a net charge as the result of charge transferring between phases^{3,7,66–68}. Moreover, even the contact between two identical materials^{69–73}, can separate charge mediated by microscopic-level fluctuations⁷⁴ (surface composition and/or structure of the material) and translated into macroscopic electrical effects. Also, charge transfer through sliding contact (triboelectrification)^{75,76}, is much faster⁷⁷ and often greater⁷⁸ than from static contact due an increase in contact area, heating and material transfer^{5,6}. In fact, a high energy state^{11,79,80}, is developed at the interface when two solids are rubbed together, bringing the interface to a non-equilibrium state, and generating a triboplasma⁸¹.

Complex mechanochemical reactions are also the source of electrostatic charges during extrusion, injection molding and other polymer manufacturing and finishing processes. Although mechanochemistry is a now considered a mature science and rapidly developing field^{82–84}, the study of mechanical forces driving chemical reactions in polymers was first carried out in the 1930s, a period in which polymers were starting to be the basis of important industrial goods⁸⁵. The use of extrusion to melt and mold plastics induces polymer chain scission⁸⁶, reducing molecular weight, viscosity, and strength⁸⁷. Moreover, bond breakage due to shear drives the formation of free radical species⁸⁸ that undergo redox reactions⁶ with the formation of electrostatic charges and can be trapped within the bulk polymer.

Many materials under strain or temperature gradients can also experience spontaneous electric polarization. Flexoelectricity^{89–91}, is an electromechanical coupling effect where charge accumulation is an instantaneous outcome of strain gradients. It is also a universal effect⁹² allowed by symmetry in any material⁹³, but polymers^{94–96}, and elastomers^{97–99}, are highly suitable to electromechanical coupling. Also, dielectrics are susceptible to charge separation during solidification or melting (thermoelectric effect)^{100,101}. Interfaces are important sites for charge buildup, but phase boundaries are moving across the material at the phase transition. Charge carriers are then also moving across the interface, but through phases with different dielectric constants (Maxwell-Wagner effect) and thus producing a charge accumulation at the interface^{102,103}. Finally, excess space charges can be trapped within the solidified material, transforming it in an electret^{104,105}.

With several sources of electrostatic charging, electrostatics is related to everyday phenomena, impacting daily life activities, industrial processes and/or routine laboratory procedures. Thus, considering the mechanisms by which insulator materials become electrified, objects produced in 3D printers through Fused Deposition Modeling (FDM) process must also spontaneously undergo the build-up of electrostatic charge. Here, we show that 3D printing brings together all the electrostatic charging characteristics described above: extrusion, friction, phase changing, strain gradient, contacting surfaces between different (polymer/substrate) and/or identical materials and, solid-liquid interfaces under temperature gradients. Despite the widespread use of FDM, there is a lack of systematic studies describing the electrostatic charging characteristics of printed objects. Preliminary results, as shown in Supplementary Information Fig. S1, confirm our initial suspicion that even small objects with a few layers of polymer can accumulate thousands of volts.

Results and Discussions

The investigation of charge buildup and dissipation in 3D printing was done employing five thermoplastics without any pigments: acrylonitrile butadiene styrene (ABS), polyethylene terephthalate glycol-modified (PETG), polylactic acid (PLA), polycaprolactam (Nylon 6),

and thermoplastic polyurethane (TPU). While all the filaments displayed charge accumulation during the 3D printing processes, the magnitude of charge on each polymer was influenced differently by printing parameters. As shown in Fig. 1a, we recall that many mechanisms are inherently associated with the 3D printing process. However, due to the viscoelastic and/or chemical nature of the melted and extruded thermoplastic, one phenomenon may be more pronounced than the other.

The polymers were printed on three different substrate that frequently appeared at distinct positions in the triboelectric series^{3,59,106–108}, float glass (soda-lime); steel and; polytetrafluorethylene (PTFE). The selection was based on the triboelectric series, where glass is typically positioned at the top and tends to acquire a predominantly positive charge after contact with other materials. PTFE is recognized for becoming negatively charged upon contact with various materials, and steel, situated in the middle of the series, tends to become either positive or negative, depending on the material it comes into contact with.

Figure 1b shows the influence of these substrates (at room-temperature) on the electrostatic potential of the objects printed. Most of the representative maps have a quasi-homogeneous electrostatic potential, predominantly negatively charged when printed on glass and positively charged for those printed on PTFE. Only the objects printed on steel display both positive and negative charges on the surface. The heterogeneous charge domains of materials printed on steel can be understood considering its position on the triboelectric series and its role as an electronic conductor substrate. The electrostatic potential maps reveal that objects often perceived as electro-neutral can exhibit significant electric potential gradients when considering adjacent pixels. Moreover, only Nylon and TPU printed in glass and steel have mappings with electrostatic potentials uniformly distributed and close to zero.

The average electrostatic potentials on the pixels of the maps are shown in Fig. 1c helps to comprehend the polarity of the objects and it was used to construct the triboelectric series seen in Fig. 1d. First, a very important generalization comes out from Fig. 1c: all objects printed on PTFE are positively charged while all objects printed on glass are negatively charged. The charge magnitude of objects printed on steel is usually low, except for PETG and PLA. As a metal conductor, steel can dissipate part of the charges accumulated by the polymers but PETG¹⁰⁹ and PLA¹¹⁰ have the characteristic to accumulate and hold electrostatic charges. ABS holds particular significance as a representative material, primarily due to its widespread use in 3D printing. Additionally, its ability to accumulate both positive (PTFE as substrate) and negative (glass as substrate) charges, ultimately reaching a net charge close to zero (steel as substrate), makes it a key filament to modulate the electrostatic charges in printed objects.

Selected spots with the highest electrostatic potentials on the printed objects were monitored over time and the results are shown in Fig. 1e. On glass, PETG and PLA maintain their potentials for extended periods, whereas Nylon, TPU, and ABS exhibit rapid charge dissipation. PETG, PLA and ABS objects keep the electrostatic potential on both steel and PTFE. As expected, the high-insulating PTFE substrate trap the charges on the printed materials, excepted for Nylon that has a linear charge decay in the first 3 h and then undergoing a steady state but at low potentials. Although, some works are intended to add fillers to Nylon to increase the electrostatic charge dissipation¹¹¹, Nylon is a hydrophilic material and tends to dissipate charges even on PTFE substrate.

Recent works have highlighted the influence of printing parameters on the mechanical and tribological properties printed bodies^{112,113}. For example, an increase in the extruder's printing temperature has been observed to initially elevate the tensile strength and elastic modulus, followed by a subsequent decline¹¹⁴. Higher tensile strength is usually obtained elevated print speeds¹¹⁵, and even the

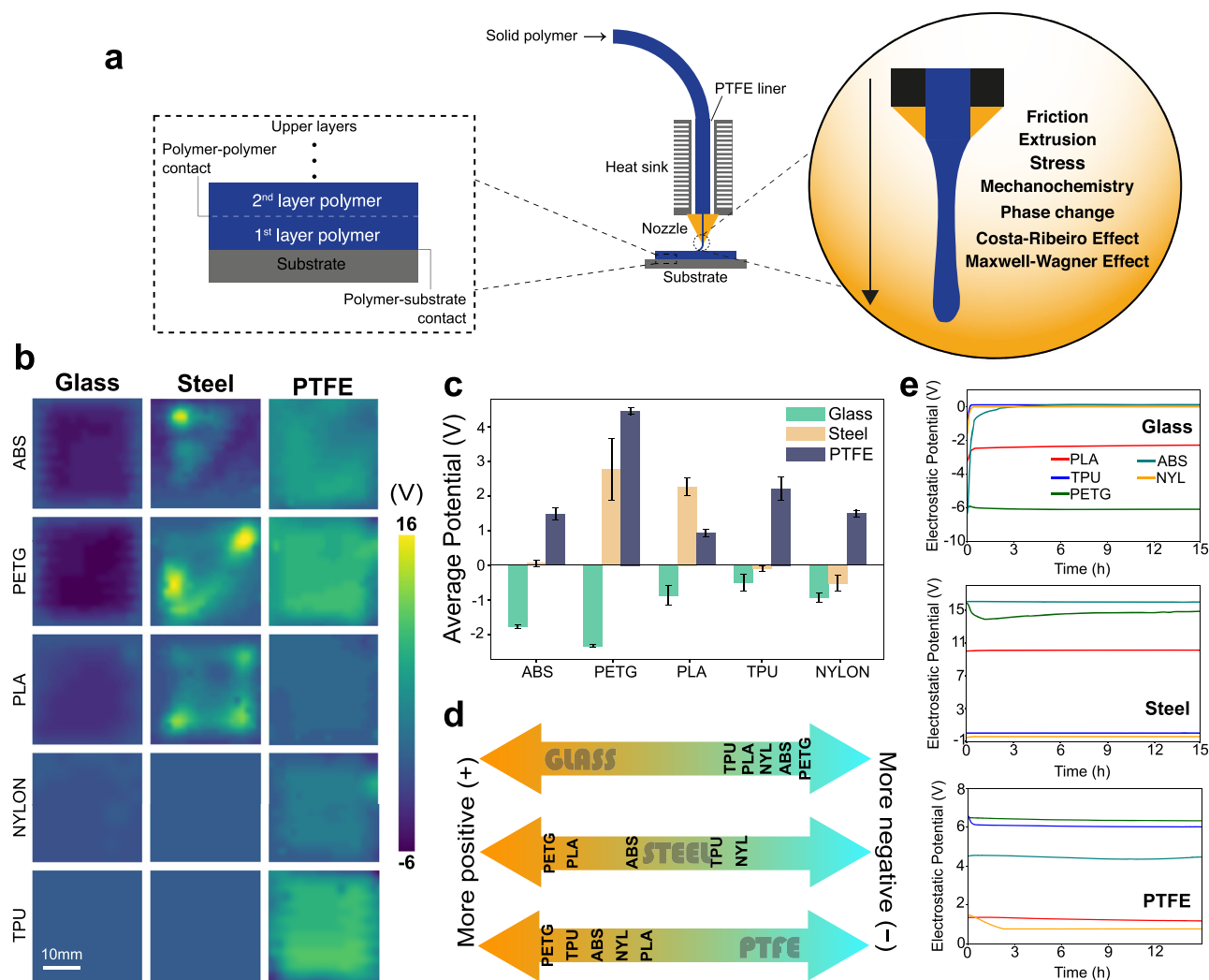


Fig. 1 | Polymer-substrate electrification. **a** Illustration of polymer electrification mechanisms observed during 3D printing. **b** Electrostatic mapping of five polymers (ABS, PETG, PLA, TPU, and Nylon) on three different substrates: glass, steel, and PTFE. **c** Average potential of pixels in each electrostatic mapping. **d** Triboelectric series depicting the electrification tendencies of five polymers on three different substrates. **e** Dissipation of the most electrified region of the samples for each

substrate. All electrostatic maps are sized at 30 mm × 30 mm and only one layer with a thickness of 0.2 mm. Objects were printed with the substrates under room-temperature. Error bars represent the standard deviation of the electrostatic potential values, averaged over at least three independent experiments per condition.

raster direction has been found to significantly influence the strength of the specimens¹⁶. Here, we also aimed to assess the effect of printing parameters on the electrostatic charge of the specimens. As seen in Fig. 2a, four printing parameters were investigated using glass as standard substrate: raster orientations (direction); print speeds; substrate temperature; and extruder temperature. The detailed procedure for printing protocols and electrostatic measurements can be found in the methods section.

The direction in which the sample is printed can drive the electrification pattern. As seen in Fig. 2b, the electrostatic potential maps show that charge accumulation is dependent on the printing direction. Although it is easier to observe the effect of concentric printing on the electrostatic potential, all other maps have features derived from the direction of printing. For example, higher electrostatic potentials are found in the corner of ABS printed diagonally. PETG displays a diagonal distribution of charge accumulation running through the center of the piece, while PLA presents a more homogeneous distribution, albeit with lower potentials at the top-left corner. Negative charges accumulate near the perimeter of ABS and PLA prints when done diagonally, but PETG undergoes charge buildup at the center.

Moreover, the vertical direction aligns negative charges perpendicularly. The average potential plot shows that the diagonal direction (which is the standard raster orientation for most printers) has the highest charge buildup on ABS and PETG, but electrostatic potential peaks are found on PLA printed in both concentric and vertical directions. As already mentioned, TPU and Nylon have fast dissipation rates (see Supporting Information Fig. S2) and their average potentials remain consistently low, with minimal influence from the printing direction. It is important to note that the experiments in Fig. 2b were conducted under identical parameters, meaning the results presented here should not be taken as general cases. As we discuss in the following paragraphs, other parameters can easily override the effect of printing direction.

Print speed is an important parameter for the quality of printed objects. Increased print speeds result in the formation of voids and other morphological defects within the printed product, affecting both its internal structure and surface quality, but having low impact on micromechanical properties¹⁷. The results seen in Fig. 2c show that at 20 mm/s, ABS buildup positive charges, while at higher speeds (80 mm/s and 140 mm/s) accumulates negative charges. At a low print

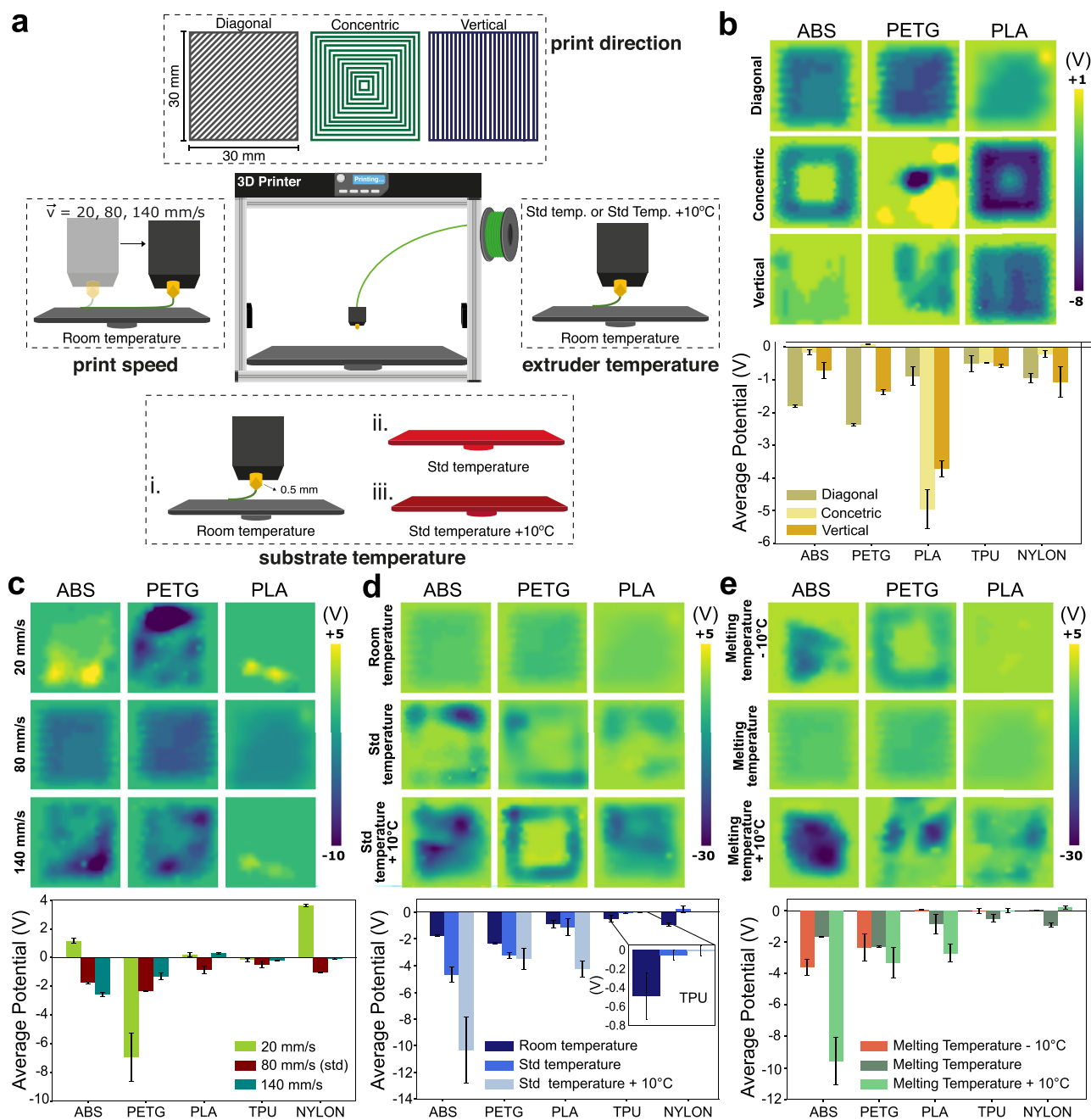


Fig. 2 | Impact of printing parameters on electrostatic charging. **a** Illustration of the tested parameters, along with representative electrostatic potential maps and average potentials for **(b)** printing direction, **(c)** print speed mappings, **(d)** substrate temperature, and **(e)** extruder temperature. All electrostatic maps are sized

at 30 mm x 30 mm and have a thickness of 0.2 mm. Error bars represent the standard deviation of the electrostatic potential values, averaged over at least three independent experiments per condition.

speed (20 mm/s) PETG has a very negative region, but a more homogeneous charge distribution is found at 80 mm/s. In fact, the moderated print speed (80 mm/s) generates the more homogeneous charge distribution for all tested materials. Such as ABS, PLA also display the feature of changing between positive and negative charges, depending on the velocity. As seen in the average potential plot there is marginal effect of velocity on TPU, but the higher positive potentials were found on Nylon under low print speed. Usually, the velocity of sliding contacts does not have a huge impact on the electrostatic charging of objects¹¹⁸, although for some cases it may lead to a reduction in the charge-to-mass ratio¹¹⁹. Here, the higher print speed also reduces charge buildup for most materials, except ABS.

As mentioned before, temperature plays a key role on 3D printing. For example, increasing the printing temperature can effectively improve the mechanical properties^{120,121}, and the quality¹¹⁵ of the material. Here, we observed that objects printed under higher temperatures (whether in the substrate or the extruder) tend to accumulate more electrical charge. Figure 2d shows that the standard objects printed using ABS, PETG or PLA on the glass substrate under room temperature display low and homogeneous electrostatic charge patterns. The electrostatic potential increases for the standard temperature of each printed material, reaching even higher potentials with a 10°C increase in the substrate temperature. Also, under elevated temperatures, electrostatic charges display a more heterogeneous

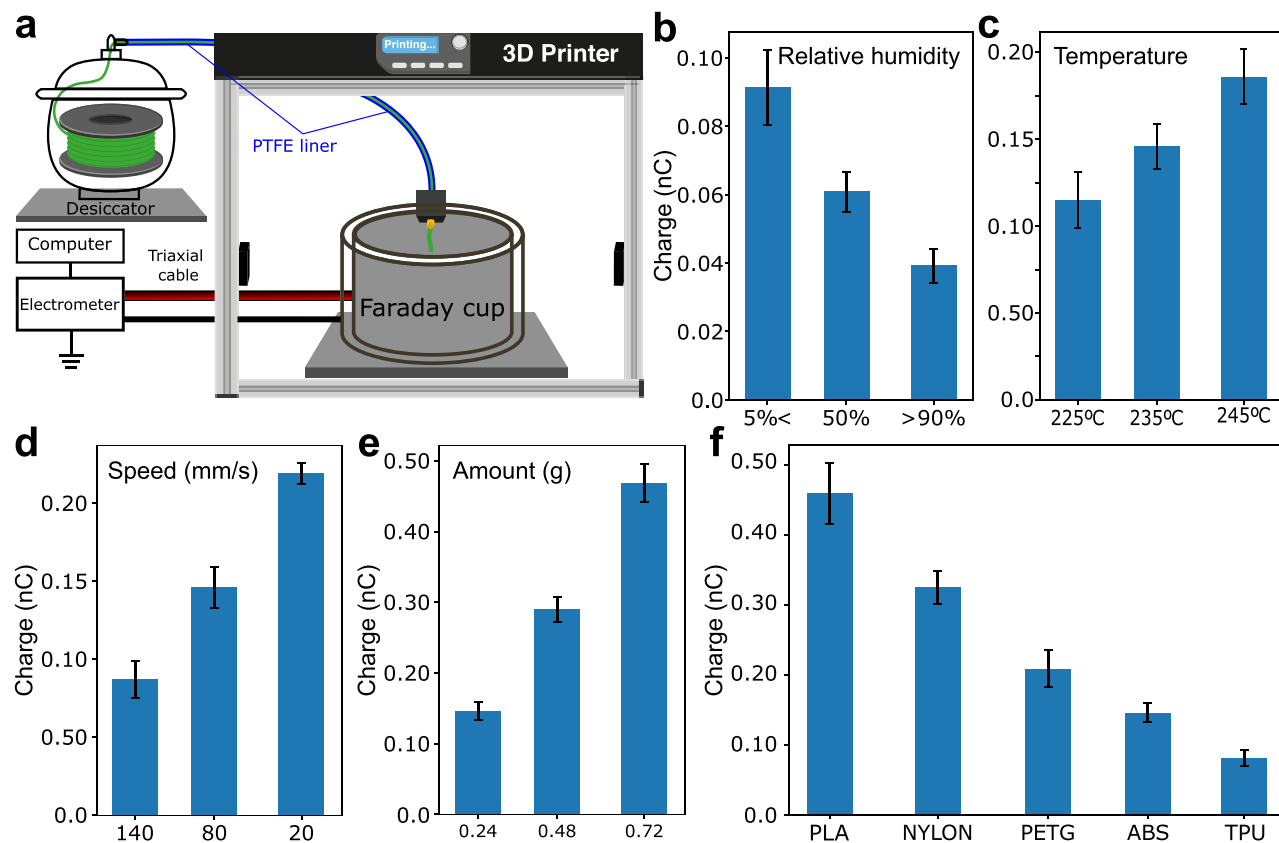


Fig. 3 | Direct charge measurement using a Faraday cup. **a** Schematic illustration of the setup used to measure the charge of extruded filaments, following 24 hour conditioning in a desiccator at controlled humidity levels. Influence of **(b)** relative humidity, **(c)** extrusion temperature, **(d)** extrusion speed, and **(e)** the amount of extruded material on the charge detected by the Faraday cup. **f** Charge acquired by

different polymer filaments after extrusion. The experiments seen in **(b–e)** used ABS as filament. Error bars represent the standard deviation of the electrostatic potential values, averaged over at least three independent experiments per condition.

distribution. Moreover, the average potential plot shows that the effect of temperature for TPU and Nylon is negligible.

The extruder temperature has a similar effect on the charging behavior of the printed objects. As seen in Fig. 2e, the melting temperature generates homogeneous potentials for all polymers, lower potentials for ABS but also a relatively low charging for PETG, PLA, TPU and Nylon. When the temperature is decreased, ABS and PETG are more electrified while PLA displays a close to zero potential map. On the other hand, negative charges are accumulated when the temperature is 10 °C higher than the melting temperature of each polymer. Moreover, as observed in the average potential graph, TPU and Nylon have electrostatic potentials oscillating close to zero volts, independent of the temperature of the extruder.

We recall that charge transfer is facilitated at higher temperatures. Usually, with an increase temperature, the interface became more excited, making it more susceptible to mediate charge transfer^{122,123}. Also, contact charging is associated with rising temperatures at the contacting junctions of sliding surfaces, forming a tribo-plasma^{75,76}. Moreover, due to the different nature of polymers, with variations in mechanical, electrical, thermal, and chemical properties, it is expected that each printing parameter will exert a unique influence on the electrostatic pattern of each printed object.

Although the wide range of results presented in Fig. 2 may seem complex due to the inherent variability of triboelectrification across different polymers, several key trends can be extracted. These trends are summarized in Table S1, which outlines the optimal printing conditions for either minimizing or maximizing electrostatic charge accumulation. This summary also helps clarify how certain variables

can dominate or even override others—for example, a high-speed print may still result in low charge if paired with vertical print direction and a heated substrate. Among all parameters studied, temperature—particularly of the substrate and extruder—emerges as the most influential factor. This is especially evident in Fig. 2d, e, where the bar scales display a broader potential range compared to other experiments, highlighting that temperature can effectively dominate the overall charge behavior regardless of other settings. Taken together, these insights establish a foundational framework to tailor the electrostatic behavior of 3D printed materials through controlled parameter tuning.

Figure 3 demonstrates how charge accumulation during extrusion is strongly influenced by environmental and process parameters Fig. 3a. illustrates how the filaments were pre-conditioned in a controlled environment before undergoing extrusion. As shown in Fig. 3b, relative humidity has a marked inverse relationship with charge buildup: filaments conditioned under low humidity (<5%) exhibited significantly higher charge levels than those at moderate (~50%) or high humidity (>90%). This supports the hypothesis that adsorbed water facilitates charge dissipation, likely by enhancing surface conductivity or acting as a mobile ion reservoir. Although controlling humidity inside the 3D printer chamber proved to be a challenging task once the printing process begins, we successfully printed materials using filaments that had been conditioned at specific humidity levels for 24 h. As shown in Fig. S3, low humidity conditions result in printed pieces with high electrostatic potential. In some cases, as illustrated in Fig. S4, filaments with excessive moisture adsorption can produce bubbles that burst during extrusion—a well-known issue in polymer processing. These defects lead to irregular printed pieces,

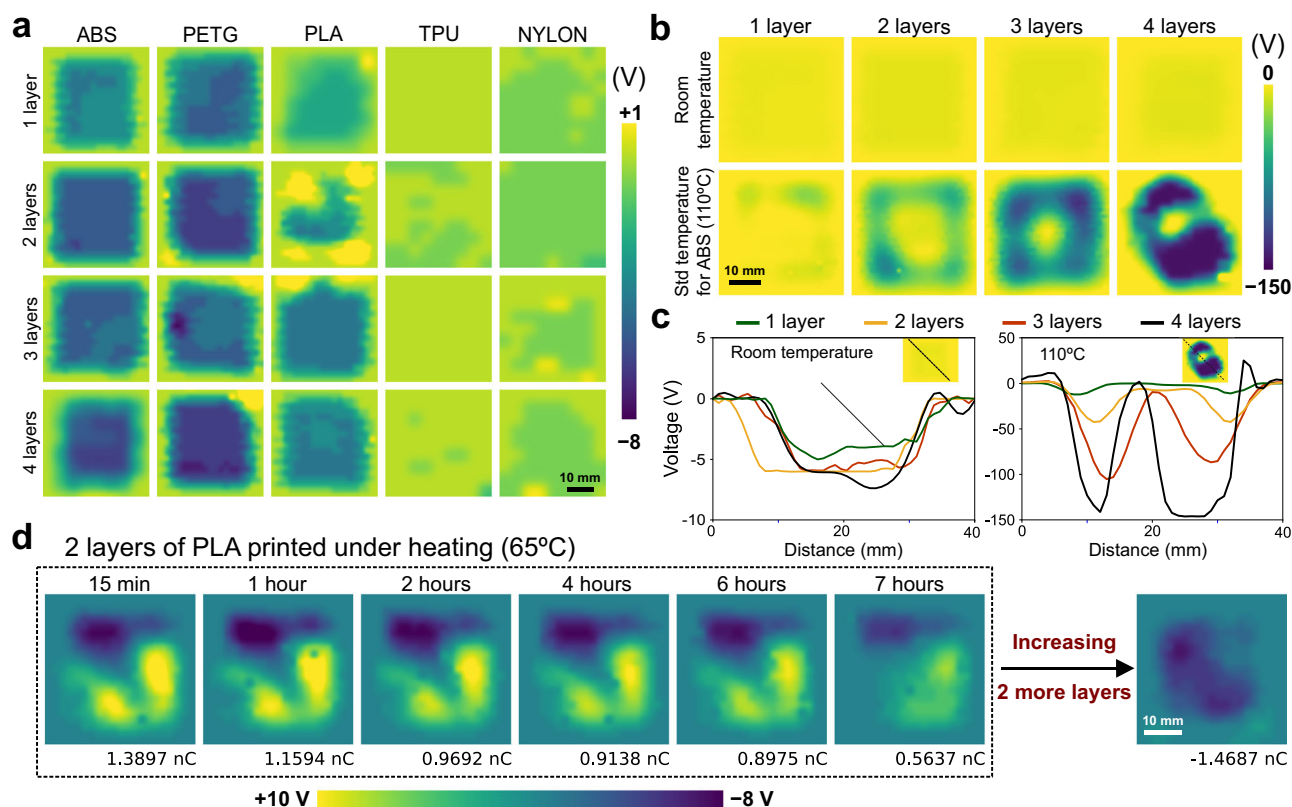


Fig. 4 | Polymer-polymer electrification analysis. **a** Electrostatic mappings depicting the influence of layer count (one to four layers) for the five polymers. **b** Comparison of four layers of ABS, printed at room temperature and under the standard substrate temperature. **c** Representative diagonal line profiles extracted

from the mappings shown in **(b)**. **d** Charge build-up and decay experiments showcasing 2 layers of PLA printed on top of 2 previously printed layers. All electrostatic maps are sized at 40 mm x 40 mm and each layer is 0.2 mm thick.

with the burst bubble locations often corresponding to areas of high electrostatic potential.

Temperature (Fig. 3c) also plays a pivotal role, with higher nozzle temperatures leading to greater charge accumulation. This could be attributed to increased polymer chain mobility and mechanochemical activation at elevated temperatures, enhancing charge transfer during extrusion. Interestingly, slower extrusion speeds (Fig. 3d) also correlate with higher charge levels, possibly due to prolonged contact times and increased friction between the filament and hotend surfaces. As expected, the total amount of extruded material (Fig. 3e) is directly proportional to the recorded charge, reflecting a cumulative charging process. Finally, Fig. 3f reveals material-dependent charging behavior, with PLA acquiring the highest charge, followed by Nylon, PETG, ABS, and TPU. These differences likely stem from variations in polymer polarity, chain mobility, and surface chemistry, highlighting the complex interplay of material properties with triboelectric and thermoelectric effects during 3D printing. Together, these results emphasize the importance of both environmental conditioning and printing parameters in controlling electrostatic behavior of printed materials.

Contact charging is not exclusive to dissimilar materials; identical insulating materials can also undergo tribocharging⁷⁴. For example, the direction of average charge transfer is material-dependent: for PTFE-PTFE contact, the surface with the larger contacting area charges positively, while in Nylon-Nylon contact, the surface with the larger contacting area charges negatively¹²⁴. Thus, we have printed objects with more layers to investigate the polymer-polymer electrification. Figure 4a shows representative potential maps for the polymers

printed on glass under room temperature. Charge accumulation usually increases with the number of layers, clearly observed on ABS and PETG when comparing objects with one and two layers. The number of layers does not affect TPU and Nylon but have an important effect on PLA tribocharging, linearly increasing negative potentials with the number of layers. Finally, the electrostatic potential decay in samples with one and four layers (Supporting Information Fig. S5) was further evaluated. The results indicate that with more layers the dissipation is slower, probably due to the entrapment of charges within the bulk polymer.

The effect of the number of layers on contact charging is highlighted when the substrate is heated up to the standard temperature to print ABS. As seen in Fig. 4b, ABS accumulates large amounts of negative charges on objects printed with increasing layers with regions reaching roughly -150V. In fact, ABS displays large and heterogeneous electrostatic potentials, leading to electric fields as high as 30 kV/m across adjacent spots on the polymer's surface (Fig. 4c). We have observed that positive charges can be trapped within PLA for long periods of time (Fig. 4d), while this PLA with a positive net charge induces negative potentials on subsequent layers printed atop it.

The contrasting behaviors of ABS and PLA observed in Fig. 4 can be attributed to their distinct positions in the triboelectric series and their material-specific charge transport properties. ABS typically resides in the negative region of the triboelectric series and shows a tendency to accumulate and retain negative charge after contact interactions¹⁰⁷. In contrast, PLA has been reported to develop positive surface charges, particularly in triboelectric nanogenerators, where it

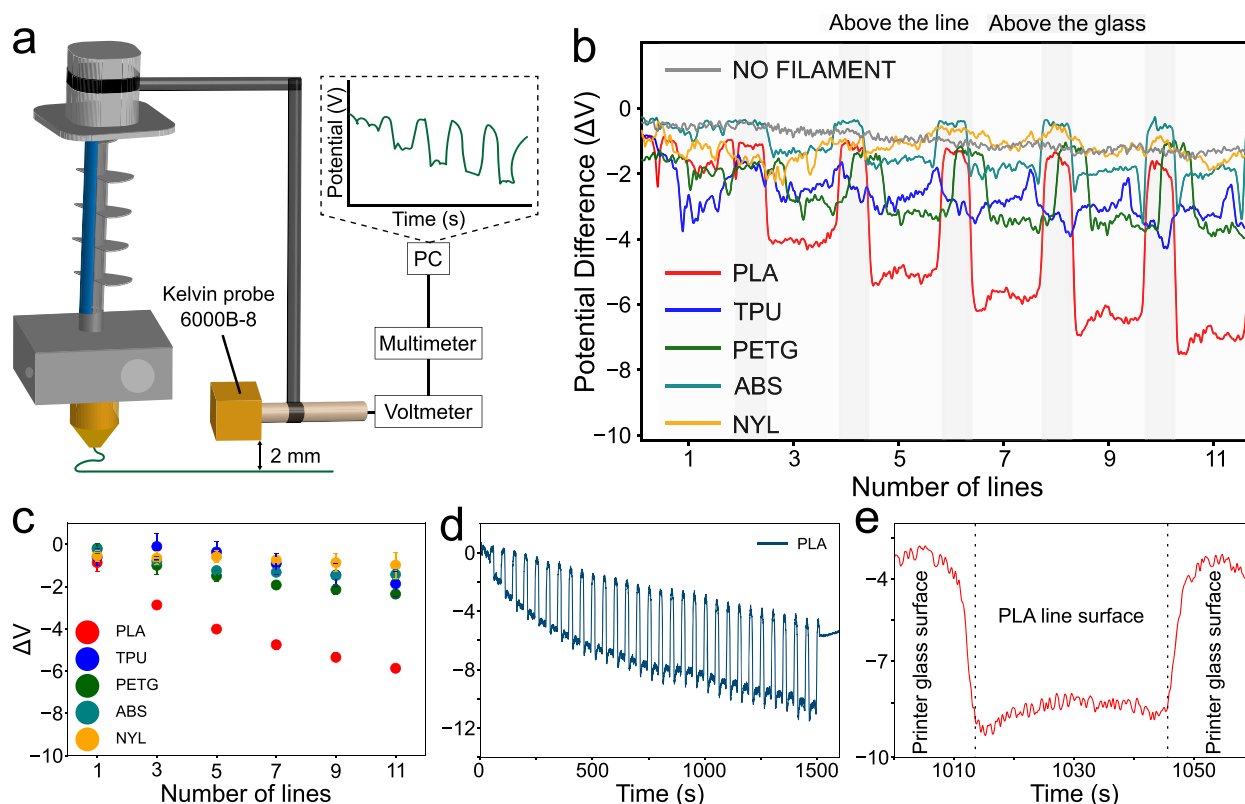


Fig. 5 | Real-time in-situ monitoring of electrification during printing.

a Experimental setup configuration. **b** Normalized potential profiles (excluding $-20V$ from the printer motor turned on) and **(c)** mean and standard deviation of the potential profiles for different polymers. **d** Visualization of 60 overlapping printed

PLA lines. **e** Close-up of the graph in **(d)**, highlighting the distinction in potential capture between the printed line and the glass surface. See Supporting Information for actual images of the setup and Supporting Movie 1.

has demonstrated efficient charge accumulation and retention¹²⁵. These intrinsic differences are reflected in our results: ABS exhibits charge stabilization with increasing layers, while PLA shows a nearly linear increase in surface potential, indicating continued charge build-up. This suggests that PLA is more responsive to polymer–polymer contact charging across layers, while ABS may be more influenced by interfacial or substrate effects.

The electrostatic potential maps analyzed thus far were recorded in situ but only after the printing process. In contrast, as schematically shown in Fig. 5a, we have now attached the Kelvin probe to the arm of the printer's hot end to enable an online, real-time survey of electrostatic charge buildup while printing a single line of extruded polymer. Due to the reciprocating nature of the printing process, the Kelvin probe only reads the potential of every other printed line—it records the first line, skips the second, records the third, skips the fourth, and so on. This is an important consideration when interpreting Fig. 4b. The electrostatic potential trends in Fig. 5b, c reveal that PLA uniquely exhibits a nearly linear increase in charge with the number of layers. This suggests that polymer–polymer electrification is significant for PLA (as it was seen in Fig. 3f), but not for most other materials. In contrast, ABS and PETG exhibit charge stabilization with subsequent layers (a behavior also observed in Fig. 3a), while TPU, initially positively charged, undergoes a polarity reversal. Nylon displays minimal electrification, aligning with the results from electrostatic potential maps. Importantly, although the charge in subsequent layers does not drastically change, it consistently becomes more negative with increasing layers. This explains why most multi-layered printed materials exhibit stronger negative potentials compared to single-layer prints. The persistent charge buildup in PLA, even after 60 overlapping layers (Fig. 5d), indicates strong interactions not only with the glass

substrate (which maintains lower potentials, as highlighted in Fig. 4e) but also with its underlayers, preventing spontaneous detachment—a behavior not observed in other tested polymers.

In addition to the Kelvin probes arrangements showed before, a common multimeter was employed for monitoring the charge during 3D printing (Fig. 6a). This simplified apparatus serves two purposes: (1) it provides a straightforward and accessible method for researchers less familiar with traditional electrostatic measurements, and (2) it enables further investigation of polymers with seemingly low charge buildup. While Kelvin probes are the gold standard for electrostatic measurements on dielectric polymers, the use of a multimeter is particularly useful in cases such as TPU and Nylon printing, where charges can dissipate rapidly at the interface. In principle, using a metallic substrate we could measure the charge transfer at the interface during printing.

The charging curves starting at the beginning of printing and stabilizing upon completion indicate electrification resulting from polymer electrification mechanisms, aligning with post-printing electrostatic mappings. After printing TPU (Fig. 6b), there is a potential decay over time, even though the system is highly insulated from the ground. Although TPU (and Nylon) did not accumulate high electrostatic potentials, they transfer large amounts of charge to the substrate. In fact, TPU has a higher maximum voltage during printing when compared to other polymers (Fig. 6c). Also, TPU samples at lower speeds exhibit higher electrification levels (Fig. 6d), with a 0.2 V difference between the lowest (20 mm/s) and highest (60 mm/s) speeds due to prolonged polymer–metal contact and, consequently, more tribocharging.

Adjusting metallic substrate and extrusion temperatures influences polymer charging (Fig. 6e, f). Higher substrate temperatures

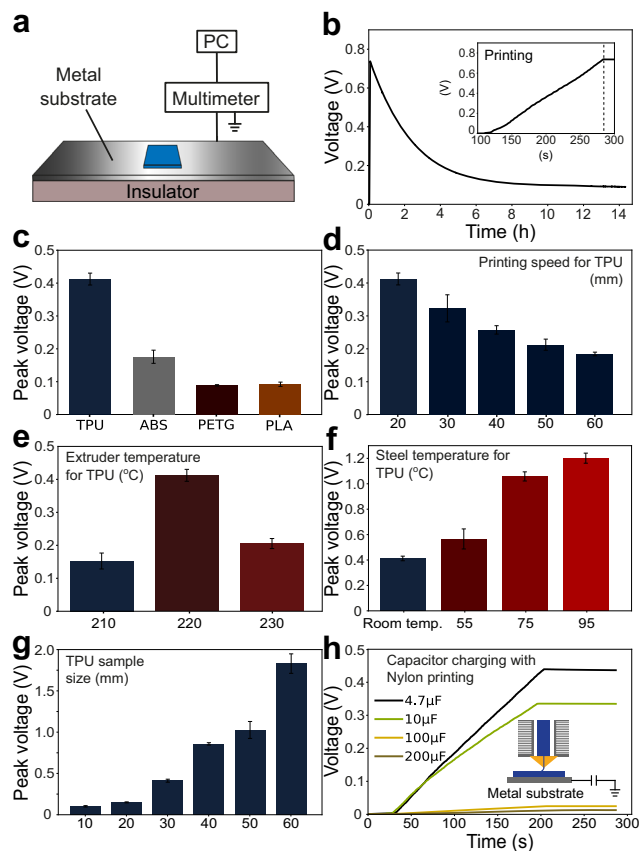


Fig. 6 | Charge transfer during TPU printing. **a** Configuration of the experimental setup. **b** Metal charging observed during printing and subsequent dissipation. **c** Presentation of average and standard deviation values of the maximum voltage during metal charging for TPU, ABS, PETG, and PLA. **d** Average and standard deviation of the maximum TPU voltage during metal charging at various printing speeds. **e** Average and standard deviation of the maximum TPU voltage during metal charging at different extrusion temperatures. **f** Average and standard deviation of the maximum TPU voltage during metal charging at different metal temperatures. **g** Average and standard deviation of the maximum TPU voltage during metal charging with varying sample sizes. **h** Ceramic capacitor charging comparison during Nylon printing on a metallic substrate.

and/or standard extrusion temperature result in greater electrification while smaller sample sizes lead to lower charging levels (Fig. 6g). Moreover, since charges are transferred from the polymer to the metal substrate, we explored the possibility of harvesting energy during 3D printing. Nylon exhibits a notably high voltage peak during printing quickly exceeding 2 V (not shown) and it was used for energy harvesting and/or charge monitoring through capacitor charging. As seen in Fig. 6h, there is a linear increase in the voltage recorded on the capacitor charging during the Nylon printing process. Finally, the setup seen in Fig. 6 introduces a novel approach to monitor and quantify electrostatic charges using regular multimeters, providing a practical and accessible method for researchers, practitioners and hobbyists that work with 3D printing.

The electrostatic potentials displayed on the printed materials can be high enough to cause electrostatic discharge (ESD)¹²⁶, mainly considering the heterogeneity of charge distribution and the electric field associated with it. ESD becomes even more significant in the context of the ongoing trend towards the downscaling of circuits^{23–27}, characterized by reductions in both size and weight. In fact, electronics, comprising intricate circuits and delicate components and do not support more than few volts¹²⁷. Thus, we developed simple and accessible

procedures to control and mitigate the electrostatic charge in printed objects. First, Zerostat piezoelectric gun (a tool commonly utilized by enthusiasts to remove electrostatic charges from vinyl records) was used to charge the substrate prior to the printing. As observed in Fig. 7a, the “U” letter printed with PLA has a close to zero-volt potential after 5 positive shots done with the Zerostat gun on the glass substrate but displaying a homogeneous positive potential with 15 positive shots.

Charge control can also be done by triboelectrification. A polyethylene (PE) film as rubbed against the glass substrate that accumulated positive charges (Fig. 7b). When TPU is printed on glass, the result is a slight positive system, but the detachment of TPU reveal a very important feature: TPU top face is positive while its bottom face is strongly negative. This means that the electrostatic potentials maps recorded in situ are underrated because image charges induced in the substrate can decrease charge on the polymers¹²⁸. In fact, electrostatic maps recorded ex situ (removing the objects from the glass substrate and supporting them on a metallic plate grounded) show that the potentials can easily reach -500 V with a few layers of ABS (Fig. 7c). This more realistic use of 3D printed materials shows that the electrification should be a significant concern when employing such objects for electronic supports or in microfluidic applications¹²⁹. Figure 7d presents an illustration (top) of the setup used to print a multi-filament sample composed of ABS, PETG, and Nylon on a textured polyetherimide (PEI) substrate. All filaments were printed using the same extruder and bed temperatures to ensure consistent thermal conditions. Also shown at the top is a photograph of the printed sample, with the corresponding electrostatic potential map displayed below. In this configuration, ABS and Nylon exhibit positive surface potentials (the later showing the highest) while PETG develops a more negative potential on the same substrate. This simple experiment highlights the value of combining electrostatic mapping with multi-material 3D printing. It offers a promising tool not only for fundamental investigations of interfacial charging phenomena but also for advancing the design of mechanically robust multi-material prints, where electrostatic interactions may contribute to improved interfacial adhesion.

To further explore the functional implications of electrostatic charging in 3D printing, we investigated the fabrication of electret materials^{130–133}, using controlled printing conditions. The electret fabrication process is illustrated in Fig. 8a, demonstrating a straightforward approach: 3D printing was conducted on a polarized metal substrate, which was subsequently grounded before electrostatic mapping. A key observation is that a metal plate polarized with a positive potential results in a negatively charged electret, and vice versa. We hypothesize that this phenomenon arises from charge induction in the filament due to the polarized substrate. As observed in other systems, a polarized surface influences the chemical activity of ions in the filament—favoring cation accumulation under negative potential and anion accumulation under positive potential.

Figure 8b presents ABS-based electrets with both positive and negative charging, while Fig. 8c shows PETG electrets. An important observation is that the electrostatic potential increases in magnitude over the first 12 h after printing, suggesting a redistribution of charge within the material. While the precise mechanism is still under investigation, we hypothesize that this effect may be linked to thermal gradients established during cooling, which could facilitate charge migration toward the surface¹³⁴. Additionally, PETG demonstrates superior charge retention compared to ABS. Under the same polarization conditions (± 200 V), PETG exhibits more homogeneous charge distribution and higher electrostatic potential.

An important trend in the triboelectric series is also reflected in the results. Polyesters, such as PETG, are typically positioned in the positive region of the triboelectric series, indicating a natural tendency to acquire positive charge. This characteristic is evident in the positive PETG electret, which not only retains charge effectively but also

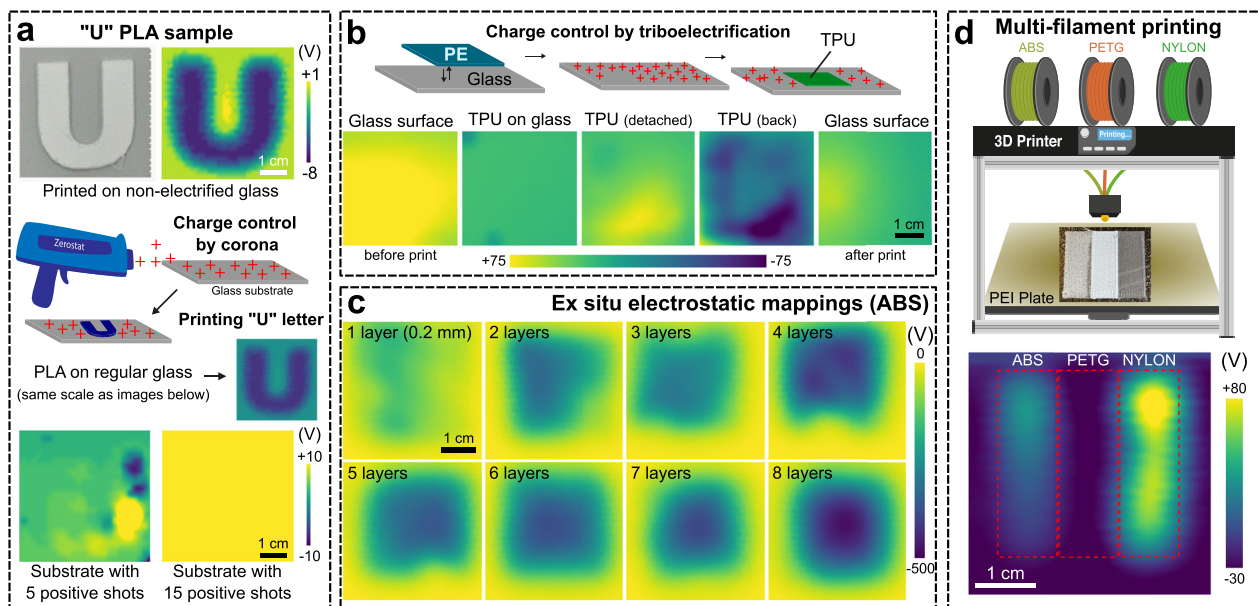


Fig. 7 | Charge control and mitigation. **a** Charge control performed with a Zerostat® piezoelectric gun applying 5 positive shots and 15 positive shots on a printed sample in the "U" shape. **b** Electrification of glass and PTFE by friction with a polyethylene plate and impression of a TPU sample on the electrified surfaces

(electrostatic mappings of PTFE see Supplementary Information Fig. S6). **c** Ex situ mapping of ABS with increasing layers. **d** Multi-filament sample composed of ABS, PETG, and Nylon, printed on a Bambu Lab textured PEI plate. Dotted red rectangles indicate the positions of the materials within the electrostatic map.

highlights the material's molecular properties that enhance its ability to trap positive charges. Another set of experiments using a different setup (Fig. S8) to produce electrets is shown in Fig. S9. Two copper tapes were applied atop the glass substrate and linked to a ± 200 V DC. The result is a homogeneous negative charged ABS material with a very slow potential dissipation. This quasi-electret is the result of trapped charges within the electric field that is facilitated during the melting/solidification process of the polymer. Water adsorption mediate negative charge buildup on polarized glass surfaces¹³⁵ and this negative charge can be transferred to the polymer during the 3D printing process.

To further probe the role of internal structure in both standard charging and electret formation, we examined the effect of infill density and print thickness on surface potential. As shown in Supplementary Fig. S10, two ABS samples with identical external geometry but differing infill densities (10% and 100%) display markedly different electrostatic behavior: the low-density structure exhibits minimal surface potential, while the fully filled sample reaches values approaching ~ 100 V. In contrast, for electret fabrication (Fig. S11), infill density appears to play a minor role. Here, the surface potential correlates more strongly with the number of printed layers. Electrets printed with five layers at 100% infill reached surface potentials near ~ 350 V, while samples with fewer layers, regardless of infill, exhibited significantly lower potentials. These electrets were printed on a positively polarized metal plate ($+500$ V) and mapped using a Trek 347 electrostatic voltmeter to capture the higher surface voltages. Together, these findings suggest that for conventional charging, infill density influences field distribution, whereas for electret applications, the overall charge-holding capacity is more dependent on the bulk material volume and interface area.

Throughout this work, we identified and systematically evaluated the key parameters governing charge accumulation during the 3D printing of polymers. First, electrostatic charging is a universal phenomenon in printed filaments, with its magnitude and polarity dependent on both environmental and printing conditions. Relative humidity and temperature were shown to significantly affect charge generation, with lower humidity and higher extrusion temperatures

promoting greater charge accumulation. Among all variables tested, temperature—particularly of the extruder and the substrate—consistently exerted the strongest influence, capable of overriding the effects of speed, print direction, and material type. Additionally, specific combinations such as vertical printing at low speed on a heated substrate were effective in minimizing charges, while diagonal or concentric patterns under elevated temperatures and low humidity conditions maximized electrostatic potentials.

It is now clear that the only outcome of a 3D printing process would be a charged material. This inevitable result brings a lot of attention to printed substrates used in electronics and other segments due the inherent risk of ESD. In fact, objects with a few layers of polymers can reach thousands of volts, but printing parameters and simple procedures such as corona charging or triboelectrification can control and/or mitigate charges. Also, the ability to monitor electrostatic charges using readily available multimeters provides a practical procedure for many users.

The ability to produce electrets directly through the 3D printing process may offer new opportunities for integrating charge functionality into additive manufacturing. Energy harvesting and sensor devices relying on charged materials for input and/or feedback systems stand to benefit significantly from this easily constructed electret. We believe that even the fundamental, long-standing, and persistent questions of electrostatics, such as the nature of charge carriers, could be addressed through 3D printing.

Methods

Materials

The thermoplastic filaments (ABS, PLA, PETG, TPU, Nylon), each with a diameter of 1.75 mm, were obtained from a local supplier (3D Lab, Brazil) and extruded through a hot nozzle (0.5 mm) using a 3D printer (S3X, Sethi 3D, Brazil). The sample areas were defined as square (30x30 mm², 40x40 mm², or 50x50 mm²), and their designs were generated using Simplify 3D software and controlled by Repetier-Host. The 3D-printing parameters were set to 0.2 mm per layer with three printing directions (diagonal, vertical, and concentric), three printing speeds (20 mm/s, 80 mm/s, and 140 mm/s), three substrate

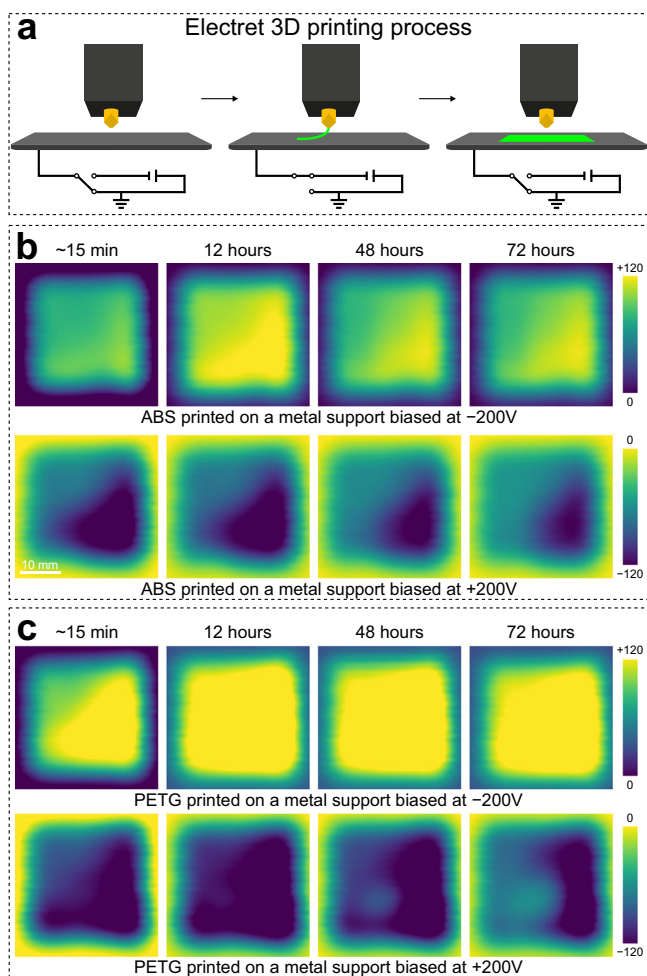


Fig. 8 | Electret production. **a** Schematic illustration of the experimental procedure for electret fabrication, where 3D printing is conducted on a polarized metal substrate (heated to the standard settings for each polymer: 110°C for ABS and 85°C for PETG), followed by grounding and electrostatic potential mapping. **b** Electrostatic potential maps of ABS-based electrets measured at 15 min, 12 h, 48 h, and 72 h after printing for both positively and negatively charged samples. **c** Electrostatic potential maps of PETG-based electrets recorded at the same time intervals, highlighting differences in charge retention and distribution between the two materials. Temperature during the experiments and the electrostatic mappings was kept the room temperature at 22–25 °C and RH was in the range of 40–50%.

temperatures, and three extruder temperatures. The substrates included glass, PTFE, and steel plates, each with a thickness of 3 mm. All printing parameters are in Supplementary Information Table 1 (TS1). Prior to experiments, the substrates were cleaned with 99.5% isopropyl alcohol (Dinâmica, Brazil) to eliminate residual electrostatic charges^{6,136}. Humidity and temperature levels were monitored using a thermo-hygrometer (KR420, Akron, Brazil).

Electrostatic potential mappings

A high-sensitivity non-contact Kelvin probe (3250, Trek, USA) with a 6.35 mm diameter was utilized for in situ electrostatic mappings conducted post-printing. The probe was connected to a voltmeter (320 C, Trek, USA), and its 20:1 voltage monitor output was measured using a multimeter equipped with an RS232 data logger. Data transmission occurred through the RS232 interface using Python-based software, which enabled real-time reading, recording, and plotting of the data. Mounted on a mechanical arm, the Kelvin probe moves in the x-y plane, driven by two NEMA17 stepping motors controlled by an

Arduino UNO R3 microcontroller (see Supporting Information Fig. S5). The system enables scanning the upper area of the sample holder at a constant height, maintaining a probe-to-surface separation of 2 mm, as recommended by the manufacturer. For mappings conducted with substrate heating, the printer was allowed to cool down to 40°C before performing the mappings due to Kelvin probe temperature limitations. The electrostatic potential mapping system can record maps with a 1 mm x 1 mm pixel resolution.

In-situ real-time measurements of electrostatic potential

A high-resolution Kelvin probe (6000B-8, Trek Inc., USA) with a 1.32 mm diameter and rapid response (<3 ms) was connected to a voltmeter (347, Trek Inc., USA), capable of measuring electrostatic potentials within the range of ± 3 kV. The voltmeter's buffered output (low-voltage replica of the measured potential) was connected to a digital multimeter (DMM, 4020, Tektronix) and recorded via an RS232 interface. Mounted on the printer arm carrying the extruder, the probe was positioned 5 mm away from the printed sample and 20 mm from the hotend, enabling real-time electrostatic potential measurements during printing. The thermoplastics were extruded in lines with a 1 mm diameter, deposited layer by layer at room temperature. (see Supporting Information Fig. S7 and Supplementary Movie 1).

Faraday cup charge measurements

Filaments were collected directly into a Faraday cup composed of two concentric metallic cylinders: the inner cup was connected to the input of an electrometer (Keithley 6514) via a low-noise triaxial cable, while the outer cup was grounded. Charge measurements were acquired using a USB-to-GPIB interface (Keithley KUSB-488B) and recorded with LabVIEW Datalogger software (NI LabVIEW 2011). Prior to the experiments, filaments were conditioned in a desiccator for at least 24 h at controlled humidity levels. Low humidity (<5%) was achieved using silica gel, high humidity (>90%) by placing water in the desiccator, and intermediate humidity (~50%) using a saturated magnesium nitrate solution.

Electret manufacturing

A metal plate (heated to the standard settings for each polymer: 110°C for ABS and 85°C for PETG), initially grounded, was used as the substrate for 3D printing. Just before the printing process began, the metal substrate was connected to a DC power source and polarized with either a positive or negative potential, depending on the desired charge of the electret. Once printing was complete, the metal plate was electrically grounded again, and electrostatic potential mapping was performed. Another set of experiments shown in Supporting Information Figs. S8 and S9 was done with copper tapes placed on glass substrate with a separation distance of 11 cm, where an object (50 mm x 50 mm x 0.8 mm) was 3D printed using ABS with the glass at room temperature. The copper tapes were connected to a DC power supply (3B Scientific, U33010-230) operating under a ± 200 V potential difference. The printing process started 60 min after turning on the DC power supply. This experimental configuration builds upon a prior finding from our group¹³⁵, demonstrating that, under an electrostatic potential difference, the glass surface becomes negatively charged at humidities higher than 30%. All the electrets were produced under ambient laboratory conditions: temperature approximately 22–25 °C (controlled by an air conditioning system) and relative humidity in the range of 40–50% (controlled by a dehumidifier – ArSec 160).

Multi-filament printing

A Bambu Lab X1 Carbon 3D printer equipped with an Automatic Material System (AMS) was used for multi-filament printing. Prior to printing, the ABS, PETG, and Nylon filaments were stored in the AMS under low humidity conditions (<5% RH) for 24 h to ensure consistent moisture content. All materials were printed using the same

parameters: a bed temperature of 100 °C, an extruder temperature of 260 °C, and a print speed of 300 mm/s. The samples were printed in a vertical direction with a single layer, using the Bambu Lab textured polyetherimide (PEI) build plate as the substrate.

Net charge calculation

Surface charge density on each pixel of the electrostatic potential mappings was calculated following a previously described procedure^{6,137}. Pixels on the surface map are squares with 1 mm sides, where virtual charges are placed. The electrostatic potential (V_T) measured 2 mm from the matrix plane is generated by all charges (q_i) weighted by the distance r from the charge to the measuring point and can be calculated using a C++ code for the equation of the principle of superposition defined as follows:

$$V_T = \sum_{i=1}^n V = \frac{1}{4\pi\epsilon_0} \sum_{i=1}^n \frac{q_i}{r_i} \quad (1)$$

The number of excess charge per pixel is adjusted by trial and error, until the calculated and measured potentials match, within experimental error. Charge density was also confirmed by using Eq. 2, which is the solution to Poisson's equation for a uniform surface charge distribution in a circle:

$$V = \frac{\sigma}{2\epsilon_0} (\sqrt{R^2 + r^2} - r) \quad (2)$$

where R is the radius of the circle, r is the distance from the surface to the Kelvin probe and σ is the charge density (Coulomb m⁻²).

Data availability

Source data are provided with this paper.

References

- Lacks, D. J. The unpredictability of electrostatic charging. *Angew. Chem. Int. Ed.* **51**, 6822–6823 (2012).
- IUPAC. Compendium of chemical terminology. In *Gold Book* 2nd edn (Blackwell Scientific Publications, 1997).
- McCarty, L. S. & Whitesides, G. M. Electrostatic charging due to separation of ions at interfaces: contact electrification of ionic electrets. *Angew. Chem. Int. Ed. Engl.* **47**, 2188–2207 (2008).
- Galembeck, F. & A. L. Burgo, T. *Chemical Electrostatics* 1st edn, Vol.230 (Springer, Cham, 2017).
- Baytekin, H. T. et al. The mosaic of surface charge. *Science* **333**, 308–312 (2011).
- Burgo, T. A. L. et al. Triboelectricity: macroscopic charge Patterns formed by self-arraying ions on polymer surfaces. *Langmuir* **28**, 7407–7416 (2012).
- Moreira, K. S., Lermen, D., da Campo, Y. A. S., Ferreira, L. O. & Burgo, T. A. L. Spontaneous mosaics of charge formed by liquid evaporation. *Adv. Mater. Interfaces* **7**, 2000884 (2020).
- Gill, E. W. B. & Alfrey, G. F. Production of electric charges on water drops. *Nature* **169**, 203–204 (1952).
- Klinkenberg, A. & van der Minne, J. L. *Electrostatics in the Petroleum Industry* (Elsevier, Amsterdam, 1958).
- Lenard, P. About the electricity of waterfalls. *Ann. Phys. (Leipz.)* **46**, 584–636 (1982).
- Heinecke, G. *Tribochemistry* (Akademie-Verlag, Berlin 1984).
- Olenick, R. P., Apostol, T. M. & Goodstein, D. L. *Beyond the Mechanical Universe: from Electricity to Modern Physics* (Cambridge University Press, 1986).
- Williams, E. R. The tripole structure of thunderstorms. *J. Geophys. Res. Atmos.* **94**, 13151–13167 (1989).
- Kudin, K. N. & Car, R. Why are water–hydrophobic interfaces charged? *J. Am. Chem. Soc.* **130**, 3915–3919 (2008).
- Ovchinnikova, K. & Pollack, G. H. Can water store charge?. *Langmuir* **25**, 542–547 (2009).
- Lacks, D. J. Frictile attraction. *Nat. Phys.* **6**, 324–325 (2010).
- Bhattacharyya, I., Maze, J. T., Ewing, G. E. & Jarrold, M. F. Charge separation from the bursting of bubbles on water. *J. Phys. Chem. A* **115**, 5723–5728 (2011).
- Kolarž, P. et al. Characterization of ions at Alpine waterfalls. *Atmos. Chem. Phys.* **12**, 3687–3697 (2012).
- Choi, D. et al. Spontaneous electrical charging of droplets by conventional pipetting. *Sci. Rep.* **3**, 1–7 (2013).
- Waitukaitis, S. R., Lee, V., Pierson, J. M., Forman, S. L. & Jaeger, H. M. Size-dependent same-material tribocharging in insulating grains. *Phys. Rev. Lett.* **112**, 218001 (2014).
- Lee, V., Waitukaitis, S. R., Miskin, M. Z. & Jaeger, H. M. Direct observation of particle interactions and clustering in charged granular streams. *Nat. Phys.* **11**, 733–737 (2015).
- Lacks, D. J. & Shinbrot, T. Long-standing and unresolved issues in triboelectric charging. *Nat. Rev. Chem.* **3**, 465–476 (2019).
- Vinson, J. E. & Liou, J. J. Electrostatic discharge in semiconductor devices: an overview. *Proc. IEEE* **86**, 399–420 (1998).
- Intel Packaging Databook. Chapter 3: ESD/EOS. <http://www.intel.com/design/packtech/packbook.htm> (2000).
- E. S. D. Association, *Fundamentals of Electrostatic Discharge: Part One—An Introduction to ESD*, EOS/ESD Association. <https://www.esda.org/esd-overview/esd-fundamentals/part-1-an-introduction-to-esd/> (2013).
- AN-40-005. *The Prevention and Control of Electrostatic Discharge (ESD)*. <https://www.minicircuits.com/app/AN40-005.pdf?srsltid=AfmBOor-OuUM6fWNY61vqHFr-7LNaMEQQG8mYIZEs4d80L4IGK2uL7> (2015).
- Kaiser, K. L. *Electrostatic Discharge* (CRC Press, Boca Raton, 2006).
- Donald, D. K. Electrostatic contribution to powder-particle adhesion. *J. Appl. Phys.* **40**, 3013–3019 (1969).
- Glor, M. Hazards due to electrostatic charging of powders. *J. Electrostat.* **16**, 175–191 (1985).
- Wang, J., Xu, Y., Li, W., Yang, Y. & Wang, F. Electrostatic potentials in gas–solid fluidized beds influenced by the injection of charge inducing agents. *J. Electrostat.* **67**, 815–826 (2009).
- Kaialy, W. A review of factors affecting electrostatic charging of pharmaceuticals and adhesive mixtures for inhalation. *Int. J. Pharm.* **503**, 262–276 (2016).
- Ermiş, E. Adhesion of food powders BT– food powders properties and characterization. In *Food Engineering Series* (ed. Ermiş, E.) 53–71 (Springer International Publishing, 2021).
- May, D. C. & Berard, D. L. Fires and explosions associated with aluminum dust from finishing operations. *J. Hazard. Mater.* **17**, 81–88 (1987).
- Gibson, N. Static electricity—an industrial hazard under control?. *J. Electrostat.* **40–41**, 21–30 (1997).
- Skinner, D., Olson, D. & Block-Bolten, A. Electrostatic discharge ignition of energetic materials. *Propellants Explos. Pyrotech.* **23**, 34–42 (1998).
- Schein, L. B. *Electrophotography and Development Physics* Revised edition, Vol. 362 (Laplacian, 1996).
- Schein, L. B. Recent progress and continuing puzzles in electrostatics. *Science* **316**, 1572–1573 (2007).
- Taylor, M. D. & Seeker, P. E. *Industrial Electrostatics: Fundamentals and Measurements* (Research Studies Pr Ltd, 1994).
- Xue, J., Wu, T., Dai, Y. & Xia, Y. Electrospinning and electrospun nanofibers: methods, materials and applications. *Chem. Rev.* **119**, 5298–5415 (2019).
- Li, X. et al. Electrospinning-based strategies for battery materials. *Adv. Energy Mater.* **11**, 2000845 (2021).
- Luraghi, A., Peri, F. & Moroni, L. Electrospinning for drug delivery applications: a review. *J. Control. Release* **334**, 463–484 (2021).

42. Kestelman, V. N., Pinchuk, L. S. & Goldade, V. A. *Electrets in engineering: fundamentals and applications*. 1st edn, Vol. 281 (Springer New York, NY, 2000).
43. Sessler, G. M. Electrets: recent developments. *J. Electrostat.* **51–52**, 137–145 (2001).
44. Wu, M.-L., Wang, D. & Wan, L.-J. Directed block copolymer self-assembly implemented via surface-embedded electrets. *Nat. Commun.* **7**, 10752 (2016).
45. Zhang, K. et al. A Gd@C82 single-molecule electret. *Nat. Nanotechnol.* **15**, 1019–1024 (2020).
46. Kawamoto, H. & Umez, S. Development of electrostatic paper separation and feed mechanism. *J. Electrostat.* **65**, 438–444 (2007).
47. Jaworek, A. et al. Hybrid electrostatic filtration systems for fly ash particles emission control. A review. *Sep. Purif. Technol.* **213**, 283–302 (2019).
48. Horn, R. G. & Smith, D. T. Contact electrification and adhesion between dissimilar materials. *Science* **256**, 362–364 (1992).
49. Lacks, D. J. & Mohan Sankaran, R. Contact electrification of insulating materials. *J. Phys. D. Appl. Phys.* **44**, 453001 (2011).
50. Sobolev, Y. I., Adamkiewicz, W., Siek, M. & Grzybowski, B. A. Charge mosaics on contact-electrified dielectrics result from polarity-inverting discharges. *Nat. Phys.* **18**, 1347–1355 (2022).
51. Kaponig, M., Mölleken, A., Nienhaus, H. & Möller, R. Dynamics of contact electrification. *Sci. Adv.* **7**, eabg7595 (2022).
52. Galembeck, F. et al. Friction, tribochemistry and triboelectricity: recent progress and perspectives. *RSC Adv.* **4**, 64280–64298 (2014).
53. Jungwirth, P. Spiers memorial lecture: ions at aqueous interfaces. *Faraday Discuss.* **141**, 9–30 (2008).
54. Yan, X. et al. Central role of bicarbonate anions in charging water/hydrophobic interfaces. *J. Phys. Chem. Lett.* **9**, 96–103 (2018).
55. Tang, Z., Lin, S. & Wang, Z. L. Quantifying contact-electrification induced charge transfer on a liquid droplet after contacting with a liquid or solid. *Adv. Mater.* **33**, 2102886 (2021).
56. Zhao, X. et al. Studying of contact electrification and electron transfer at liquid-liquid interface. *Nano Energy* **87**, 106191 (2021).
57. Lu, Y. et al. Liquid-liquid triboelectric nanogenerator based on the immiscible interface of an aqueous two-phase system. *Nat. Commun.* **13**, 5316 (2022).
58. Miljkovic, N., Preston, D. J., Enright, R. & Wang, E. N. Electrostatic charging of jumping droplets. *Nat. Commun.* **4**, 2417 (2013).
59. Burgo, T. A. L., Galembeck, F. & Pollack, G. H. Where is water in the triboelectric series? *J. Electrostat.* **80**, 30–33 (2016).
60. Lin, S., Xu, L., Chi Wang, A. & Wang, Z. L. Quantifying electron-transfer in liquid-solid contact electrification and the formation of electric double-layer. *Nat. Commun.* **11**, 399 (2020).
61. Sun, M., Lu, Q., Wang, Z. L. & Huang, B. Understanding contact electrification at liquid–solid interfaces from surface electronic structure. *Nat. Commun.* **12**, 1752 (2021).
62. Ober, P. et al. Liquid flow reversibly creates a macroscopic surface charge gradient. *Nat. Commun.* **12**, 4102 (2021).
63. Lin, S., Zhu, L., Tang, Z. & Wang, Z. L. Spin-selected electron transfer in liquid–solid contact electrification. *Nat. Commun.* **13**, 5230 (2022).
64. Healy, T. W. & Fuerstenau, D. W. The isoelectric point/point-of-zero-charge of interfaces formed by aqueous solutions and non-polar solids, liquids, and gases. *J. Colloid Interface Sci.* **309**, 183–188 (2007).
65. Gouveia, R. F. & Galembeck, F. Electrostatic charging of hydrophilic particles due to water adsorption. *J. Am. Chem. Soc.* **131**, 11381–11386 (2009).
66. Zhang, J., Coote, M. L. & Ciampi, S. Electrostatics and electrochemistry: mechanism and scope of charge-transfer reactions on the surface of tribocharged insulators. *J. Am. Chem. Soc.* **143**, 3019–3032 (2021).
67. Heinert, C., Sankaran, R. M. & Lacks, D. J. Electrostatic charge generation on material surfaces from the evaporation of liquids. *J. Electrostat.* **105**, 103450 (2020).
68. Heinert, C., Sankaran, R. M. & Lacks, D. J. Microscale bipolar charge distributions on surfaces after liquid wetting and evaporation in an electric field. *Langmuir* **37**, 8007–8013 (2021).
69. Lowell, J. & Truscott, W. S. Triboelectrification of identical insulators. II. *Theory Furth. Exp. J. Phys. D. Appl. Phys.* **19**, 1281 (1986).
70. Siu, T., Cotton, J., Mattson, G. & Shinbrot, T. Self-sustaining charging of identical colliding particles. *Phys. Rev. E* **89**, 52208 (2014).
71. Yoshimatsu, R., Araújo, N. A. M., Wurm, G., Herrmann, H. J. & Shinbrot, T. Self-charging of identical grains in the absence of an external field. *Sci. Rep.* **7**, 39996 (2017).
72. Xu, C. et al. Contact-electrification between two identical materials: curvature effect. *ACS Nano* **13**, 2034–2041 (2019).
73. Angus, J. C. & Greber, I. Contact charge transfer between nominally identical materials. *Ann. Phys.* **533**, 2000571 (2021).
74. Apodaca, M. M., Wesson, P. J., Bishop, K. J. M., Ratner, M. A. & Grzybowski, B. A. Contact electrification between identical materials. *Angew. Chem. Int. Ed.* **49**, 946–949 (2010).
75. Burgo, T. A. L., Silva, C. A., Balestrin, L. B. S. & Galembeck, F. Friction coefficient dependence on electrostatic tribocharging. *Sci. Rep.* **3**, 2384 (2013).
76. Burgo, T. A. L. & Erdemir, A. Bipolar tribocharging signal during friction force fluctuations at metal-insulator interfaces. *Angew. Chem. - Int. Ed.* **53**, 12101–12105 (2014).
77. Zhou, Y. S., Li, S., Niu, S. & Wang, Z. L. Effect of contact- and sliding-mode electrification on nanoscale charge transfer for energy harvesting. *Nano Res.* **9**, 3705–3713 (2016).
78. Ireland, P. M. The role of changing contact in sliding triboelectrification. *J. Phys. D. Appl. Phys.* **41**, 25305 (2008).
79. Camara, C. G., Escobar, J. V., Hird, J. R. & Putterman, S. J. Correlation between nanosecond X-ray flashes and stick-slip friction in peeling tape. *Nature* **455**, 1089–1092 (2008).
80. Liu, C. & Bard, A. J. Chemical redox reactions induced by cryptoelectrons on a PMMA surface. *J. Am. Chem. Soc.* **131**, 6397–6401 (2009).
81. Matta, C. et al. On the possible role of triboplasma in friction and wear of diamond-like carbon films in hydrogen-containing environments. *J. Phys. D. Appl. Phys.* **42**, 75307 (2009).
82. Do, J.-L. & Friščić, T. Mechanochemistry: A force of synthesis. *ACS Cent. Sci.* **3**, 13–19 (2017).
83. Mateti, S. et al. Mechanochemistry: A force in disguise and conditional effects towards chemical reactions. *Chem. Commun.* **57**, 1080–1092 (2021).
84. O'Neill, R. T. & Boulatov, R. The many flavours of mechanochemistry and its plausible conceptual underpinnings. *Nat. Rev. Chem.* **5**, 148–167 (2021).
85. Feldman, D. Polymer history. *Des. Monomers Polym.* **11**, 1–15 (2008).
86. Staudinger, H. & Leupold, E. O. Über isopren und Kautschuk, 18. Mitteil. Viscositäts-untersuchungen an balata. *Ber. der Dtsch. Chem. Ges. (A B Ser.)* **63**, 730–733 (1930).
87. Krusenbaum, A., Grätz, S., Tigineh, G. T., Borchardt, L. & Kim, J. G. The mechanochemical synthesis of polymers. *Chem. Soc. Rev.* **51**, 2873–2905 (2022).
88. Willis-Fox, N., Rognin, E., Aljohani, T. A. & Daly, R. Polymer mechanochemistry: manufacturing is now a force to be reckoned with. *Chem* **4**, 2499–2537 (2018).
89. Narvaez, J., Vasquez-Sancho, F. & Catalan, G. Enhanced flexoelectric-like response in oxide semiconductors. *Nature* **538**, 219–221 (2016).

90. Mizzi, C. A., Lin, A. Y. W. & Marks, L. D. Does flexoelectricity drive triboelectricity?. *Phys. Rev. Lett.* **123**, 116103 (2019).
91. Arias, I., Catalan, G. & Sharma, P. The emancipation of flexoelectricity. *J. Appl. Phys.* **131**, 20401 (2022).
92. Das, S. et al. Enhanced flexoelectricity at reduced dimensions revealed by mechanically tunable quantum tunnelling. *Nat. Commun.* **10**, 537 (2019).
93. Yudin, P. V. & Tagantsev, A. K. Fundamentals of flexoelectricity in solids. *Nanotechnology* **24**, 432001 (2013).
94. Cao, J., Piedrahita, C. & Kyu, T. Mechano-electrical conversion in highly ionic conductive solid-state polymer electrolyte membranes. *Macromol. Mater. Eng.* **304**, 1–7 (2019).
95. Šutka, A. et al. Contact electrification between identical polymers as the basis for triboelectric/flexoelectric materials. *Phys. Chem. Chem. Phys.* **22**, 13299–13305 (2020).
96. Lorenzetti, E. et al. Flexoelectric characterization of dielectrics under tensile, compressive, and flexural loads by non-contact Kelvin probe measurements. *J. Appl. Phys.* **129**, 204502 (2021).
97. Marvan, M. & Havránek, A. Flexoelectric effect in elastomers. *Relatsh. Polym. Struct. Prop.* **36**, 33–36 (2007).
98. Burgo, T. A. L., Batista, B. C. & Galembeck, F. Electricity on rubber surfaces: a new energy conversion effect. *ACS Omega* **2**, 8940–8947 (2017).
99. Santos Da Campo, Y. A. et al. Electromechanical coupling in elastomers: a correlation between electrostatic potential and fatigue failure. *Phys. Chem. Chem. Phys.* **23**, 26653–26660 (2021).
100. Costa Ribeiro, J. On the thermo-dielectric effect. *Acad. Bras. Cienc.* **22**, 325–347 (1950).
101. Gross, B. Theory of thermodielectric effect. *Phys. Rev.* **94**, 1545–1551 (1954).
102. Wagner, K. W. Erklärung der dielektrischen nachwirkungsvorgänge auf grund maxwellscher vorstellungen. *Arch. Für Elektrotechnik* **2**, 371–387 (1914).
103. Kuriakose, M., Longuemart, S., Depriester, M., Delenclos, S. & Sahraoui, A. H. Maxwell-Wagner-Sillars effects on the thermal-transport properties of polymer-dispersed liquid crystals. *Phys. Rev. E* **89**, 22511 (2014).
104. Latham, J. & Mason, B. J. Electric charge transfer associated with temperature gradients in ice. *Proc. R. Soc. Lond. A* **260**, 523–536 (1961).
105. Eyerer, P. Electric charge separation and charge storage during phase changes in the absence of external electric fields: thermoelectric effect (costa Ribeiro effect) and workman-Reynolds effect. *Adv. Colloid Interface Sci.* **3**, 223–273 (1972).
106. Diaz, A. F. & Felix-Navarro, R. M. A semi-quantitative tribo-electric series for polymeric materials: the influence of chemical structure and properties. *J. Electrostat.* **62**, 277–290 (2004).
107. Zou, H. et al. Quantifying the triboelectric series. *Nat. Commun.* **10**, 1–9 (2019).
108. Zou, H. et al. Quantifying and understanding the triboelectric series of inorganic non-metallic materials. *Nat. Commun.* **11**, 1–7 (2020).
109. Yin, J. & Nysten, B. Contact electrification and charge decay on polyester fibres: a KPFM study. *J. Electrostat.* **96**, 16–22 (2018).
110. Jaseem, S. M. & Ali, N. A. Antistatic packaging of carbon black on plastizers biodegradable polylactic acid nanocomposites. *J. Phys. Conf. Ser.* **1279**, 12046 (2019).
111. Arigbabowo, O. K. & Tate, J. S. Additive manufacturing of polyamide nanocomposites for electrostatic charge dissipation applications. *Mater. Sci. Eng. B* **271**, 115251 (2021).
112. Gunasekaran, K. N., Aravinth, V., Muthu Kumaran, C. B., Madhan-kumar, K. & Pradeep Kumar, S. Investigation of mechanical properties of PLA printed materials under varying infill density. *Mater. Today Proc.* **45**, 1849–1856 (2021).
113. Rouf, S. et al. 3D printed parts and mechanical properties: Influencing parameters, sustainability aspects, global market scenario, challenges and applications. *Adv. Ind. Eng. Polym. Res.* **5**, 143–158 (2022).
114. Tang, C. et al. Effect of process parameters on mechanical properties of 3D printed PLA lattice structures. *Compos. Part C. Open Access* **3**, 100076 (2020).
115. Ansari, A. A. & Kamil, M. Effect of print speed and extrusion temperature on properties of 3D printed PLA using fused deposition modeling process. *Mater. Today Proc.* **45**, 5462–5468 (2021).
116. Khosravani, M. R., Berto, F., Ayatollahi, M. R. & Reinicke, T. Characterization of 3D-printed PLA parts with different raster orientations and printing speeds. *Sci. Rep.* **12**, 1016 (2022).
117. Loskot, J. et al. Influence of print speed on the microstructure, morphology, and mechanical properties of 3D-printed PETG products. *Polym. Test.* **123**, 108055 (2023).
118. Zeghloul, T., Neagoe, M. B., Prawatya, Y. E. & Dascalescu, L. Triboelectrical charge generated by frictional sliding contact between polymeric materials. *IOP Conf. Ser. Mater. Sci. Eng.* **174**, 12002 (2017).
119. Trigwell, S., Biris, A. S., Sims, R. A. & Mazumder, M. K. Effects of powder velocity and contact materials on tribocharging of polymer powders for powder coating applications. *Part. Sci. Technol.* **26**, 145–157 (2008).
120. Grasso, M., Azzouz, L., Ruiz-Hincapie, P., Zarrelli, M. & Ren, G. Effect of temperature on the mechanical properties of 3D-printed PLA tensile specimens. *Rapid Prototyp. J.* **24**, 1337–1346 (2018).
121. Hsueh, M.-H. et al. Effects of printing temperature and filling percentage on the mechanical behavior of fused deposition molding technology components for 3 d printing. *Polymers* **13**, 2910 (2021).
122. Lin, S., Xu, L., Tang, W., Chen, X. & Wang, Z. L. Electron transfer in nano-scale contact electrification: Atmosphere effect on the surface states of dielectrics. *Nano Energy* **65**, 103956 (2019).
123. Xu, C. et al. On the electron-transfer mechanism in the contact-electrification effect. *Adv. Mater.* **30**, 1706790 (2018).
124. Pham, R., Virnelson, R. C., Sankaran, R. M. & Lacks, D. J. Contact charging between surfaces of identical insulating materials in asymmetric geometries. *J. Electrostat.* **69**, 456–460 (2011).
125. Shi, X., Si, W., Zhu, J. & Zhang, S. Boosting the electrical performance of PLA-based triboelectric nanogenerators for sustainable power sources and self-powered sensing. *Small* **20**, 2307620 (2024).
126. Ferreira, L. O. & Burgo, T. A. L. Suppressing and controlling electrostatic charge in micropipetting. *J. Electrostat.* **106**, 103453 (2020).
127. Li, X. et al. 28 nm CMOS process ESD protection based on diode-triggered silicon controlled rectifier. *Solid. State Electron.* **137**, 128–133 (2017).
128. Siek, M., Adamkiewicz, W., Sobolev, Y. I. & Grzybowski, B. A. The influence of distant substrates on the outcome of contact electrification. *Angew. Chem. - Int. Ed.* **57**, 15379–15383 (2018).
129. Waheed, S. et al. 3D printed microfluidic devices: enablers and barriers. *Lab Chip* **16**, 1993–2013 (2016).
130. Gong, S., Zhang, B., Zhang, J., Wang, Z. L. & Ren, K. Biocompatible poly(lactic acid)-based hybrid piezoelectric and electret nanogenerator for electronic skin applications. *Adv. Funct. Mater.* **30**, 1908724 (2020).
131. Zhu, J. et al. More than energy harvesting in electret electronics-moving toward next-generation functional system. *Adv. Funct. Mater.* **33**, 2214859 (2023).
132. Zhao, X. J., Wang, H. L., Wang, Z. L. & Wang, J. Nanocomposite electret layer improved long-term stable solid-liquid contact triboelectric nanogenerator for water wave energy harvesting. *Small* **20**, 2310023 (2024).

133. Endo, T. et al. Facile preparation and charge retention mechanism of polymer-based deformable electret. *Soft Matter* **20**, 5800–5809 (2024).
134. Rychkov, D., Yablokov, M. & Rychkov, A. Chemical and physical surface modification of PTFE films—an approach to produce stable electrets. *Appl. Phys. A* **107**, 589–596 (2012).
135. Paiva, V. T. C., Santos, L. P., da Silva, D. S., Burgo, T. A. L. & Galembeck, F. Conduction and excess charge in silicate glass/air interfaces. *Langmuir* **35**, 7703–7712 (2019).
136. Francisco, K. R., Burgo, T. A. L. & Galembeck, F. Tribocharged polymer surfaces: solvent effect on pattern formation and modification. *Chem. Lett.* **41**, 1256–1258 (2012).
137. Burgo, T. A. et al. Electric potential decay on polyethylene: role of atmospheric water on electric charge build-up and dissipation. *J. Electrostat.* **69**, 401–409 (2011).

Acknowledgements

This work is supported by Brazilian agencies MCTIC/CNPq (465452/2014-0), FAPESP (INOMAT: 2014/50906-9 and MAFN: 2025/01483-2) and CAPES—Finance Code 001 through INCT/INOMAT (National Institute for Complex Functional Materials) and MCT/Finep/CT-Infra 02/2010.

Author contributions

E.L. contributed with experimental work, data treatment, the discussion of results. Y.A.S.C. contributed with experiments and data treatment. M.A.F.N contributed with experimental work and data treatment. T.A.L.B. is the supervisor, participated in experimental design and some experiments, discussion, interpretation, and writing.

Competing interests

The authors declare no competing interests.

Additional information

Supplementary information The online version contains supplementary material available at <https://doi.org/10.1038/s41467-025-61566-8>.

Correspondence and requests for materials should be addressed to Thiago A. L. Burgo.

Peer review information *Nature Communications* thanks Farhina Haque, Soaik Im and the other, anonymous, reviewer(s) for their contribution to the peer review of this work. A peer review file is available.

Reprints and permissions information is available at <http://www.nature.com/reprints>

Publisher's note Springer Nature remains neutral with regard to jurisdictional claims in published maps and institutional affiliations.

Open Access This article is licensed under a Creative Commons Attribution-NonCommercial-NoDerivatives 4.0 International License, which permits any non-commercial use, sharing, distribution and reproduction in any medium or format, as long as you give appropriate credit to the original author(s) and the source, provide a link to the Creative Commons licence, and indicate if you modified the licensed material. You do not have permission under this licence to share adapted material derived from this article or parts of it. The images or other third party material in this article are included in the article's Creative Commons licence, unless indicated otherwise in a credit line to the material. If material is not included in the article's Creative Commons licence and your intended use is not permitted by statutory regulation or exceeds the permitted use, you will need to obtain permission directly from the copyright holder. To view a copy of this licence, visit <http://creativecommons.org/licenses/by-nc-nd/4.0/>.

© The Author(s) 2025